

Title: Elastic-plastic wave profiles in
cyclotetramethylene tetranitramine crystals

Author(s): J. J. DICK, jjd@lanl.gov
D. E. HOOKS, dhooks@lanl.gov
R. MENIKOFF, rtm@lanl.gov
A. R. MARTINEZ, armartinez@lanl.gov

Submitted to: Journal of Applied Physics

Elastic-plastic wave profiles in cyclotetramethylene tetranitramine crystals

J. J. Dick, D. E. Hooks, R. Menikoff, and A. R. Martinez
Los Alamos National Laboratory
Los Alamos, New Mexico 87545

(Dated: March 5, 2004)

The explosive molecular crystal cyclotetramethylene tetranitramine (HMX) was studied in three orientations in a set of plate impact experiments; the orientations studied were $\{110\}$, $\{011\}$ and $\{010\}$ in $P2_1/n$ space group. The elastic-plastic shock response was measured using laser interferometry. The measured particle velocity profiles showed elastic precursor decay typical of a stress relaxing material. There is anisotropy in elastic shock strength and decay. The amount of precursor decay with propagation distance and stress relaxation behind the elastic shock varied among the orientations. The $\{010\}$ orientation had larger elastic precursors than the other two orientations; the $\{010\}$ crystal does not have the regular plastic deformation mechanisms available to it. Elastic Hugoniot were obtained from the measurements. The inelastic deformation mechanisms may vary with orientation.

PACS numbers: 62.20.Fe, 62.50.+p, 81.40.Lm

I. INTRODUCTION:

Elastic precursor decay in explosive crystals has been studied for more than two decades. Most of the previous studies were on pentytritol tetranitrate (PETN) [1–3]. Strong anisotropy in the response in PETN was noted. The precursor decay anisotropy correlated with anisotropy of shock initiation of detonation. It was hypothesized that the anisotropy was due to steric hindrance to shear in these molecular crystals. The orientations that had weak hindrance to shear had weak precursors and weak decomposition reactions, while the orientations that had strong hindrance to shear and increased molecular deformation in the shear had strong elastic precursors and underwent shock initiation [3–5]. It seemed of interest to extend this study to another explosive crystal to see if this behavior occurs in more than one case. PETN is an aliphatic molecule in a tetragonal crystal and HMX, a heterocyclic molecule, is monoclinic in the beta phase.

II. EXPERIMENTAL TECHNIQUE

Plane shock experiments were performed on HMX crystals with final shock strengths of about 1.5 GPa and 2.4 GPa obtained using a light-gas gun facility. The layout of the plate impact experiments is shown in Fig. 1. Particle velocity vs time histories were recorded at the HMX/window interface using a VISAR (Velocity Interferometer System for Any Reflector). The HMX crystals were mounted on the aluminum-coated anvil disc 50.8 mm in diameter with a silicone elastomer. It was deemed important to not impact the crystals directly in order to avoid spurious effects at the impact face. The elastomer filled in any pits or scratches so that the likelihood of a significant ignition hot spot was greatly reduced. The aluminum coating on the anvil disk was

deemed important to maintain consistency with all previous experiments. The coating provides an equipotential, grounded surface to prevent any local charge buildup induced by piezoelectricity or dielectric breakdown [6]. The impactors for all experiments were 2024 aluminum. For the experiments at 1.5 GPa and an impactor velocity of about 0.315 mm/ μ s, the anvils were x-cut quartz; for the 2.4 GPa experiments at about 0.52 mm/ μ s the anvils were Kel-F [7]. Kel-F was chosen because it is a close shock impedance match to HMX. However, at 1.5 GPa x-cut quartz was used to obtain a sharp input shock to HMX, since the wave front in Kel-F has viscoelastic rounding at this stress level. The window material was polymethylmethacrylate (PMMA, Mil. Spec. P-5425D, preshrunk).

The crystal slabs were cut from larger crystals using a low-speed, diamond wheel or wire saw. Identification of crystal planes was achieved by comparison of interfacet angles measured with a protractor with calculated angles until unique agreement was obtained. Lateral dimensions of the slabs were 8 to 13 mm. The crystals were polished using a series of polishing sheets consisting of alumina down to 1 μ m embedded in plastic. Liquid detergent (Alconox) and water were used as the lubricant and carrier for removed HMX. The crystals were water-clear and inspected with a binocular microscope at magnifications up to 50x to make sure that the interiors were free of inclusions and other visible defects larger than about 2 microns. Crystal slices were viewed between crossed polarizers to ensure that the samples were not twinned. Crystals were grown by Howard Cady or the authors by slow evaporation from acetone solution.

For VISAR studies PMMA windows 12.7 mm in both diameter and thickness were bonded to the sample with the elastomer. PMMA was chosen as the window material since it is a calibrated window with shock impedance closest to HMX. It is of lower impedance, so it sends a rarefaction back into the HMX. Typically glue bond thick-

ness was $5 \mu\text{m}$. The roughened surface of the PMMA adjacent to the crystal was coated with a nonspecular aluminum mirror for VISAR particle velocity measurements. The lateral sides of the crystal and window were surrounded by an impedance-matching mixture of epoxy and 40 vol% silica to minimize edge effects (Fig. 1).

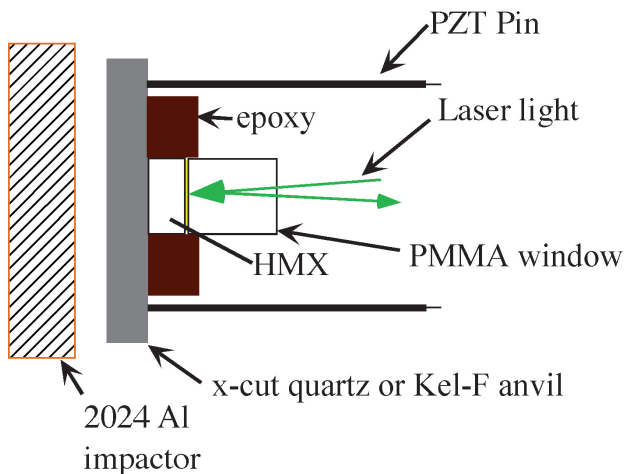


FIG. 1: Schema of the gun impact experiment with VISAR instrumentation.

Piezoelectric pins were emplaced on the rear surface of the anvil disc adjacent to the crystal. The average arrival time for a pair of diametrically placed pins is a measure of arrival time in the sample center assuming a plane wave. The time difference between arrival time at the sample center measured by the pins and the shock arrival signal recorded by VISAR yields a transit time and velocity through the crystal. The difference in signal travel times to the digitizing oscilloscopes for the two types of signals is accounted for. Shots 1067 through 1168 used two PZT pins to measure the time of arrival. Subsequent shots used 4 pins.

The measurement system used was a dual, push-pull, VISAR system [8]. The dual VISAR with different fringe constants removes ambiguity in determining the particle-velocity jump at the shock when extra fringes must be added. The light was transported from the laser to the target and thence to the interferometer table with fiber optics. The fiber optic probe on the target was obtained from Valyn International. The light interference signals were converted to voltage using photomultiplier tubes with rise and fall times of about 1 ns. The signals were recorded on digitizers at 1 or 2-ns sampling rates. Judging by the Lissajous figures generated by combining the signals that are 90° out of phase, the overall response time of the system is about 3 ns at the shock-wave arrival time.

Typical measurement errors stem from several sources. Thickness measurements for the crystal specimens and anvils were typically $\pm 2.5 \mu\text{m}$ and glue bond thicknesses were typically $5 \mu\text{m}$. PZT pin arrival times, which sig-

nal the shock arrival at the front surface of the crystal specimen and therefore form the basis for the transit time measurement, were taken at a certain level above the baseline systematically. The random error associated with this technique was estimated to be ± 2.5 ns for each pin. The timing errors associated with the VISAR measurement are due mainly to the rise time of the photomultiplier tubes, which is a systematic error of about 3ns. Combining the timing errors associated with linear measurement errors and glue bonds and the timing errors associated with the PZT pins and the VISAR itself results in a total estimated timing error of ± 12 ns. This error was propagated into the error in shock velocity for each experiment. The uncertainty in determining the elastic precursor amplitude at the crystal/window interface is about 5 m/s. This corresponds to an approximate standard deviation in longitudinal stress of 0.023 GPa.

III. EXPERIMENTAL RESULTS

Wave profiles and wave speeds were recorded for the elastic and plastic (inelastic) waves in three orientations, $\{110\}$ and $\{011\}$ and $\{010\}$ in space group $P2_1/n$. Experiments were performed on samples 1.03 to 4.66 mm thick with input stresses of about 1.5 and 2.4 GPa. Elastic precursor shock amplitude vs wave propagation distance was measured; plastic wave rise time was obtained. Note that the word plastic is used loosely to describe the following wave that accommodates the permanent deformation; the deformation in the wave may be by traditional plastic mechanisms or by brittle mechanisms depending on orientation.

A. Precursor decay

1. 1.5 GPa

The wave profiles obtained are shown in Figs. 2, 3, and 4. There is an elastic shock followed by a plastic or inelastic wave. Decay of the elastic shock strength with propagation distance as well as particle-velocity relaxation behind the shock are evident. The elastic shock strengths at a given distance of propagation are similar for the $\{110\}$ and $\{011\}$ orientations but higher for the $\{010\}$ orientation. There are also differences in wave profile with orientation. At about 3 mm and $0.75 \mu\text{s}$ propagation the $\{011\}$ orientation profile shows substantial relaxation, whereas the $\{110\}$ orientation appears to have reached steady state. The $\{010\}$ orientation decays slowly with relatively mild relaxation; the amount of relaxation is about the same at all distances observed. The measured profile is the profile at the interface and reflects properties of both the HMX crystal and the PMMA window. It represents the profile of the wave propagated through the crystal after it has interacted with the window material. The PMMA window has a viscoelastic

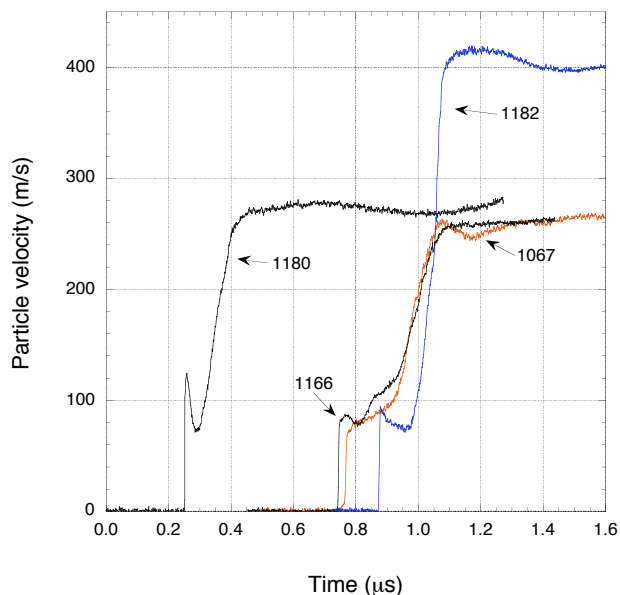


FIG. 2: Elastic precursor decay for 1.5 and 2.4 GPa shocks parallel to a $\{110\}$ plane. The profiles are those measured at the HMX/PMMA interface. At 1.5 GPa the profiles are for samples 1.23, 3.21 and 3.18 mm thick; at 2.4 GPa 3.57 mm.

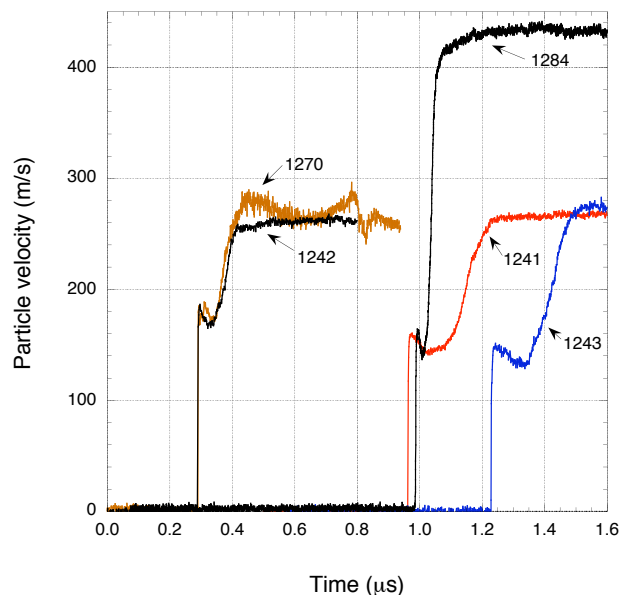


FIG. 4: Elastic precursor decay for 1.5-GPa shocks parallel to a $\{010\}$ plane. The profiles are those measured at the HMX/PMMA interface. The profiles are for samples 1.03, 1.04, 3.49, and 4.40 mm thick; at 2.4 GPa 3.65 mm.

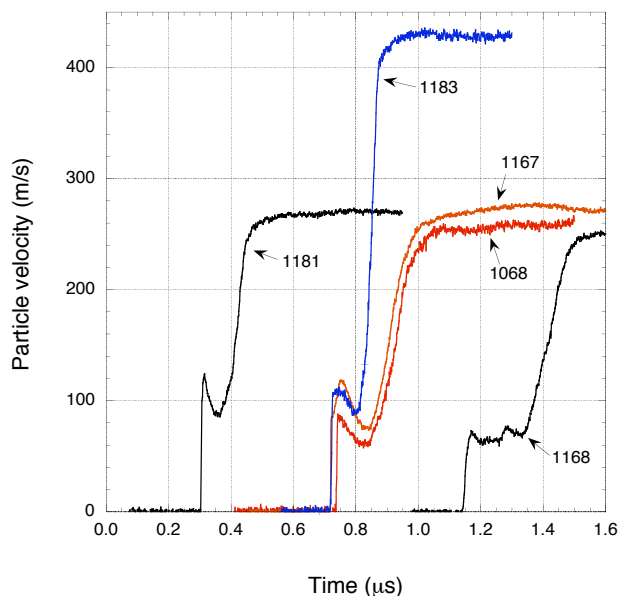


FIG. 3: Elastic precursor decay for 1.5 and 2.4 GPa shocks parallel to a $\{011\}$ plane. At 1.5 GPa the samples are 1.39, 3.00, 3.04, and 4.66 mm thick; at 2.4 GPa 3.11 mm.

response that can distort the relaxation profile [9]. Shot 1167 for $\{011\}$ orientation has a peak behind the elastic shock front, whereas other experiments show immediate relaxation behind the front. This anomalous result is not understood. There is a smaller similar effect in Shot 1270 for $\{010\}$ orientation.

2. 2.4 GPa

Elastic shock amplitude at a given crystal thickness is increased by higher input stress for $\{110\}$ and $\{011\}$ orientations. This is seen in Fig. 3 where one can compare elastic shock stresses at nearly the same thickness. At 2.4 GPa the elastic shock is decaying from a higher elastic impact stress. The approach to equilibrium is changed by increased impact stress consistent with a stress-relaxing model [1, 10, 11]. For the $\{110\}$ case the profile for a 3.57 mm sample at 2.4 GPa has relaxation behind the elastic shock, whereas the 1.5 GPa profiles at 3.2 mm do not. In $\{010\}$ orientation the elastic shock stress at about 3.5 mm propagation distance appears to have no stress dependence. This may indicate a yield process different from that observed in the other two orientations. For the $\{010\}$ experiment at 2.4 GPa the decay behind the elastic shock is very rapid; yet it relaxes to the same level as the 1.5 GPa shot.

3. decay summary

Comparison of the precursor decay with distance for the three orientations is displayed in Fig. 5. The figure shows clearly that behavior of the elastic precursor shock decay is identical for $\{110\}$ and $\{011\}$ orientations. The $\{010\}$ orientation has higher elastic precursors at large propagation distance and a lower rate of decay than the others. It is notable that $\{010\}$ starts from a lower input stress. The elastic input stress is calculated by impedance

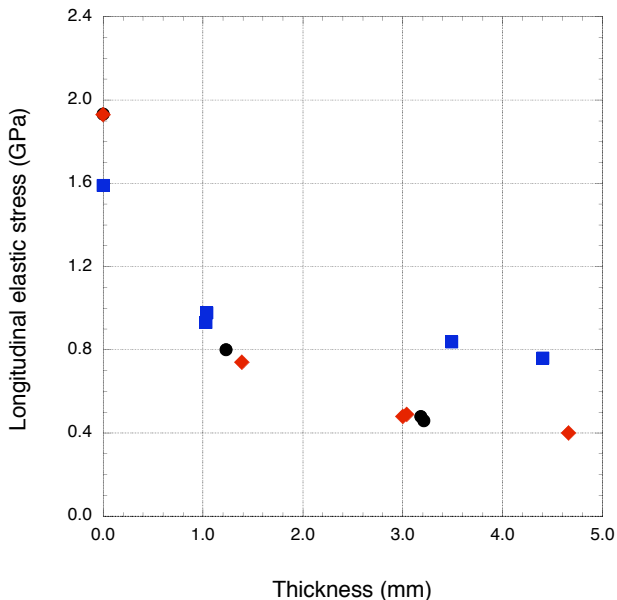


FIG. 5: Elastic stress in HMX for 1.5-GPa shocks for all orientations. The circles are for $\{110\}$ crystals, the diamonds are for $\{011\}$ crystals, and the squares are for $\{010\}$ crystals. Stresses at 0 mm are calculated stresses for an initial totally elastic response.

matching using the elastic Hugoniot deduced from the experiments. The $\{010\}$ orientation has lower elastic shock speeds (cf. Table I) and a softer Hugoniot resulting in a lower input stress. This elastic input stress is based on the assumption that the initial material response is totally elastic.

B. wave speeds with orientation; elastic Hugoniots

As the elastic wave propagates it decays in longitudinal stress, particle velocity, and wave velocity. For $\{110\}$ the mean wave velocity decays from about 4.9 to 4.2 mm/ μ s going from 1.2 to 3.2-mm-thick sample. For $\{011\}$ it decays from about 4.5 to 4.1 mm/ μ s going from 1.4 to 4.7 mm thickness. It is worthwhile to examine the variation of elastic shock speed with shock particle velocity and with orientation. These results are displayed in Fig. 6. This is consistent with a nonlinear elastic Hugoniot; the wave velocity is higher at higher stresses closer to the input face of the crystal. The elastic shock speeds are shown for the three orientations along with measured longitudinal sound speeds. One can see that the $\{110\}$ and $\{011\}$ Hugoniots are indistinguishable. A fit to the data for elastic velocity vs particle velocity for $\{110\}$ and $\{011\}$ orientations is $U=3.70+7.9u$; standard errors of the fit are 0.10 and 1.5, respectively. A longitudinal sound speed 3.74 mm/ μ s was used in the fit. There is one data point, shot 1180, at 4.86 mm/ μ s for a $\{110\}$ crystal 1.23 mm thick that is an outlier, not used in the fit. It

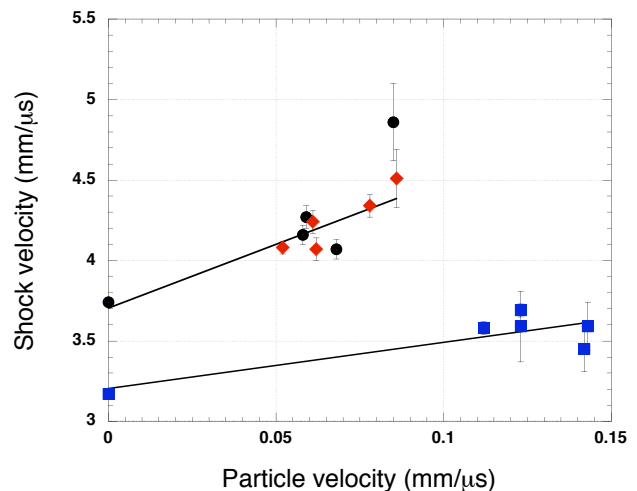


FIG. 6: Elastic wave velocity in HMX vs. particle velocity for the three orientations. The circles are for $\{110\}$ crystals, the diamonds are for $\{011\}$ crystals, and the squares are for $\{010\}$ crystals. Sound velocities measured by a pulse echo technique are included.

was found that the quartz anvil used in that experiment was up to 13 μ m thinner at the edge than in the middle. The PZT pins are about 18 mm out from the center; this led to an error in transit time measurement. For $\{010\}$ orientation the fit is $U=3.20+2.9u$; standard errors of the fit are 0.11 and 0.92. The large coefficient of the particle velocity for the $\{110\}$ and $\{011\}$ data indicates much stronger nonlinearity for the elasticity of these orientations than for $\{010\}$.

The longitudinal sound speeds were measured for the three orientations of HMX using an ultrasonic technique for measuring transit time using 10 MHz x-cut quartz crystals. The measured elastic wave speeds for $\{110\}$ and $\{011\}$ are nearly identical and considerably faster than for $\{010\}$ orientation HMX crystals. The measured longitudinal sound speeds for $\{110\}$, $\{011\}$, and $\{010\}$ are 3.76, 3.72, and 3.17 mm/ μ s, respectively.

It is interesting to compare the measured longitudinal sound speed for $\{010\}$ orientation HMX to that inferred from the incomplete elastic constant measurements of Joe Zaig [12] obtained by inelastic light scattering. His value for the elastic constant C_{22} of 26.9 GPa yields a longitudinal sound speed along the $[010]$ direction of 3.76 mm/ μ s, over 18% larger than our ultrasonic value; his provisional value is greater than the elastic shock speeds measured for this orientation. His measurements were all in the (010) plane implying no direct measurement of C_{22} . According to our calculations the longitudinal sound speeds inferred for $[110]$ and $[011]$ directions from the elastic constants are about 18% lower than our ultrasonic values that are consistent with the measured shock speeds. It must be noted that these directions are not normal to the planes with the same indices.

C. plastic wave behavior

The rise time of the plastic wave increases with propagation distance indicating unsteady behavior; the wave is not yet steady. In the case of 011 orientation the rise time increases from about 80 to 180 ns as the wave propagates from 1.4 to 4.7 mm. Steadiness is achieved when the tendency to shock up (steepen) is balanced by the dissipation of the inelastic deformation processes. For {011} orientation at about 3.1 mm, the rise time decreases from about 120 ns to 50 ns when the input stress is increased from 1.5 to 2.4 GPa. Over all the rise times are shorter for {010}. In PETN it has been suggested based on numerical modeling that conventional deformation processes of dislocation slip are active for crystal orientations that have low elastic precursors [13], orientations that do not have significant steric hindrance to shear. In a hindered orientation with large elastic precursors the modeling results compared to experimental data of Ref. 3 indicated another deformation mechanism is occurring, possibly brittle failure. Note that plastic waves normal to the {010} face in HMX have lower wave velocities than the other two orientations. The larger elastic precursors, shorter plastic-wave rise times, and slower plastic-wave velocities for {010} orientation may signify a deformation mechanism operative different from that for the other orientations studied.

In {110} and {011} orientations the final particle velocity level behind the plastic wave appears to decay with propagation distance. This may be an effect of stress relaxation associated with the precursor decay. Note that the rounding and ramp in interface particle velocity at the top of the plastic wave may be due to the viscoelastic behavior of the PMMA window material as well as its changing index of refraction as the wave profile propagates through it [14]. A viscoelastic relaxation time constant for PMMA of 0.25 μ s was given by K. W. Schuler and J. W. Nunziato [9].

D. Shock-wave tabular results

Table I lists the experimental conditions and measured quantities. Since the elastic shock is decaying as it propagates, the shock slows down as the wave decays since HMX is nonlinearly elastic. This was the case in explosive crystals of PETN also [3]. The shock velocity computed from the measured transit time and sample thickness is some mean value of the wave velocity over the propagation distance. The final velocity where the wave profile is measured is less than this mean value. Using a stress relaxing model Halleck and Wackerle estimated the error in the case of PETN to be 3.5% for a 3 GPa elastic impact stress on a 5-mm-thick sample [1].

The elastic particle velocity and longitudinal stress in HMX are computed from the intersection of the Rayleigh line given by the initial density times the mean elastic shock velocity and its reflection through the

HMX/PMMA interface state in the stress vs particle velocity plane. This approximation to the HMX release isentrope is a good one for these particle velocities that are small relative to the sound speed. This stems from the fact that the isentrope and Hugoniot have a 3rd order contact and that the fractional change in acoustic impedance given by $2s\Delta P/K_0$ is small; here s is the slope of the U-u Hugoniot, ΔP is the pressure change between the in-material elastic state and the interface state, and K_0 is the bulk modulus equal to about 15 GPa for HMX [15]. Since the pressure change is much smaller than the bulk modulus the approximation is justified; the estimated error is 1-2%. For PMMA a quadratic equilibrium Hugoniot was used: $U=2.774 + 2.182u - 2.014u^2$. Using Schuler's instantaneous Hugoniot [16] yields values 1.4% higher for the particle velocity and stress in HMX. This is less than our error estimates for the experiments.

The plastic wave rise time appears to increase with propagation distance, indicating unsteadiness. The plastic wave speed given in Table I is the Lagrangian wave velocity at half maximum. Since the wave is unsteady it does not represent the velocity of the entire wave.

IV. DISCUSSION OF THE RESULTS

The data show clearly that there is anisotropy in the strength and elastic precursor shock decay of HMX crystals. This can be understood in broad outline by examining the relationship of the plane and direction of deformation for the possible deformation mechanisms relative to the impact plane. This is summarized in Table II. The two dislocation slip planes are those observed by D. B. Sheen and J. N. Sherwood [17]. The slip directions were those proposed based on energetics of shortest Burgers vector. The twin and fracture planes have been characterized [18, 19]. The twin direction was proposed by Armstrong [20].

In an isotropic material the maximum resolved shear stress will be at 45 degrees to the impact plane; in an anisotropic material the resolved shear stress on particular crystallographic planes may be calculated through the elastic constants in a tensor analysis [21]. For impact parallel to the [110] plane we see that one slip system, the twin system and the fracture plane are available near 45 degrees to the impact plane. For the (011) plane the same slip system and the twin system are available, but the fracture plane is not. It turns out that this slip system and twin system are identical. In contrast for (010) the planes and directions for slip and twinning are all at 90 degrees to the impact plane and not available for deformation. Only the fracture system is available at 57 degrees to the (010) impact plane. Experiments were performed on {110} and {011} orientations first since these were the largest facets of the available crystals [22]. Then the observation was made that the {010} orientation would not have the primary slip systems or twinning system available. Experiments bore out that this led to

TABLE I: Results of VISAR Tests for Three Orientations of HMX Crystal

Shot num.	Sample type ^a	Thick-ness (mm)	Impactor u_I (mm/ μ s)	HMX/PMMA		Elastic precursor			Plastic wave	
				Interface u (mm/ μ s)	U_S^b (mm/ μ s)	u_p^c (mm/ μ s)	P_x^c (MPa)	U_S^d (mm/ μ s)	Rise Time (ns)	
1180	110	1.23	0.3185	0.123	4.86	0.085	790	3.48	91	
1067	110	3.21	0.3170	0.080	4.16	0.058	460	3.28	122	
1166	110	3.18	0.3068	0.083	4.27	0.059	480	3.19	133	
1182 ^e	110	3.57	0.5209	0.094	4.07	0.068	530	3.39	74	
1181	011	1.39	0.3160	0.121	4.51	0.086	740	3.26	79	
1068	011	3.00	0.3140	0.086	4.07	0.062	480	3.21	123	
1167	011	3.04	0.3141	0.085	4.24	0.061	490	3.32	118	
1168	011	4.66	0.3132	0.072	4.08	0.052	400	3.26	179	
1183 ^e	011	3.11	0.5204	0.109	4.34	0.078	640	3.65	47	
1242	010	1.04	0.3103	0.186	3.59	0.143	978	2.74	52	
1270	010	1.03	0.3158	0.182	3.45	0.142	932	2.75	87	
1241	010	3.49	0.3089	0.160	3.59	0.123	838	3.10	107	
1243	010	4.40	0.3097	0.146	3.58	0.112	760	3.08	110	
1284 ^e	010	3.65	0.5176	0.162	3.69	0.123	864	3.50	30	

^a This is the crystallographic plane in space group $P2_1/n$ that was impacted. The impact plane is parallel to this plane.

^b This shock velocity is computed from the sample thickness divided by the transit time. It represents a mean velocity through the sample.

^c Values were calculated from the intersection of the Rayleigh line given by the initial density times the mean elastic shock velocity and its reflection through the interface state.

^d These are Lagrangian wave velocities.

^e These experiments used Kel-F anvils; all others used x-cut quartz.

high elastic precursors. This appears to confirm the importance of conventional deformation mechanisms in this weak, brittle, molecular crystal. Apparently, the conventional mechanisms of plastic flow, i. e., dislocations and twins, are still operative in the orientations $\{110\}$ and $\{011\}$. In bcc iron it has been suggested that the stress relaxation may be due to twinning and the equilibrium stress or Hugoniot elastic limit is controlled by dislocation processes [23]. For $\{010\}$ orientation the deformation may be brittle failure, possibly using the fracture planes $\{011\}$. It is worth noting that increasing the impact stress does not appear to increase the precursor amplitude at a given propagation distance for this orientation. Impact stress dependence is expected for stress-relaxing behavior associated with dislocation processes.

In PETN anisotropy in elastic precursor strength correlated with anisotropy in shock initiation sensitivity. The orientations with high elastic precursors underwent exothermic decomposition more readily. The mechanism for the sensitivity is not known, although there are several possibilities. In PETN the sensitive orientations had steric hindrance to shear along available slip planes, whereas the insensitive orientations did not [3, 4]. A shear-induced change of conformer as the mechanism for the increased sensitivity has been proposed by Gruzdkov

and Gupta [24]. A chemical pathway for decomposition based on spectroscopic investigations was proposed by Dreger, et. al. [25]. A change in deformation mechanism may be involved. Theoretical work toward describing the behavior of explosive crystals is progressing [26–31]. A review of many HMX physical properties is given in Ref. [32]. Although the mechanism for the initiation of decomposition chemistry has not been determined, we suspect that the behavior we have observed should be common in molecular explosives. Experiments to explore the possible anisotropy of shock initiation sensitivity in HMX crystals are underway.

Acknowledgments

The experiments were performed with the help of Bob Medina and Joe Lloyd. Helpful conversations with Dr. Mike Winey at WSU are appreciated. This work was performed under the auspices of the U. S. Department of Energy and partially supported by the Office of Munitions Memo of Understanding between the Department of Energy and the Department of Defense.

[1] P. M. Halleck and Jerry Wackerle, J. Appl. Phys. **47**, 976 (1976).

[2] L. Soulard, Thesis, L'Universite de Haute-Alsace, 1990;

TABLE II: Analysis of angle between deformation system and shock plane.

Shock plane	Deformation type	Deformation plane	Interplanar angle deg	Deformation direction deg	Angle ^a deg
[110]	slip1	(001)	79	[100]	90
	slip2	(101)	45	[10 $\bar{1}$]	56
	twin	(101)	45	[10 $\bar{1}$]	56
	fracture	(011)	64	-	-
[011]	slip1	(001)	33	[100]	90
	slip2	(101)	51	[10 $\bar{1}$]	56
	twin	(101)	51	[10 $\bar{1}$]	56
	fracture	(011)	0	-	-
[010]	slip1	(001)	90	[100]	90
	slip2	(101)	90	[10 $\bar{1}$]	90
	twin	(011)	90	[10 $\bar{1}$]	90
	fracture	(011)	57	-	-

^a This is the angle between the shock plane and the deformation direction.

- L. Soulard and F. Bauer, in *Shock Compression of Condensed Matter-1989*, edited by S. C. Schmidt, J. N. Johnson, and L. W. Davison (Elsevier, Amsterdam, 1990), p. 817.
- [3] J. J. Dick and J. P. Ritchie, *J. Appl. Phys.* **76**, 2726 (1994).
- [4] J. J. Dick, *J. Appl. Phys.* **81**, 601 (1997).
- [5] D. Spitzer, Ph. D. thesis, Universite Louis Pasteur de Strasbourg, p. 153, 1993.
- [6] R. A. Graham and W. J. Halpin, *J. Appl. Phys.* **39**, 5077 (1968).
- [7] Kel-F is the 3M Company brand name for polytrifluorochlorethylene.
- [8] Willard F. Hemsing, *Rev. Sci. Instrum.* **50**, 73 (1979).
- [9] K. W. Schuler and J. W. Nunziato, *Rheol. Acta* **13**, 265 (1974).
- [10] J. N. Johnson and O. E. Jones, *J. Appl. Phys.* **41**, 2330 (1970).
- [11] Y. M. Gupta, *J. Appl. Phys.* **46**, 3395 (1975).
- [12] J. Zaug, *Eleventh International Symposium on Detonation* (Office of Naval Research, Arlington, VA, 1998), p. 498.
- [13] J. M. Winey and Y. M. Gupta, in *13th APS Topical Conference on Shock Compression of Condensed Matter* (2003).
- [14] Ralph Menikoff, manuscript in preparation (2004).
- [15] R. Menikoff and T. D. Sewell, *High Pressure Research* **21**, 121 (2001).
- [16] K. W. Schuler, *J. Mech. Phys Solids* **18**, 277 (1970).
- [17] D. B. Sheen, J. N. Sherwood, H. G. Gallagher, A. H. Littlejohn, and A. Pearson, Final Report to the U. S. Office of Naval Research, 'An Investigation of Mechanically Induced Lattice defects in Energetic Materials,' (University of Strathclyde, Glasgow, 1993), pp. 53 ff.
- [18] S. J. P. Palmer and J. E. Field, *Proc. R. Soc. kA* **383**, 399 (1982).
- [19] H. H. Cady in *Structure and Properties of Energetic Materials*, edited by D. H. Liebenberg, R. W. Armstrong, and J. J. Gilman, (Materials Research Society, Pittsburgh, 1982), p. 243.
- [20] R. W. Armstrong, H. L. Ammon, Z. Y. Du, W.L.L. Elban, and X. J. Zhang, *ibid.*, p. 227.
- [21] J. N. Johnson, *J. Appl. Phys.* **43**, 2074 (1972).
- [22] J. J. Dick and A. R. Martinez, in *Shock Compression of Condensed Matter-2001*, edited by M. D. Furnish, N. N. Thadani, and Y. Horie (American Institute of Physics, 2002), p. 817.
- [23] J. N. Johnson and R. W. Rohde, *J. Appl. Phys.* **42**, 4171 (1971).
- [24] Y. A. Gruzdkov and Y. M. Gupta, *J. Phys. Chem. A* **2000**, 11169 (2000).
- [25] Z. A. Dreger, Y. A. Gruzdkov, Y. M. Gupta, and J. J. Dick, *J. Phys. Chem. A* **2002**, 247 (2002).
- [26] E. J. Reed, J. D. Joannopoulos, and L. E. Fried, *Phys. Rev. B*, **62**, 16500, (2000).
- [27] D. Margetis, E. Kaxiras, M. Eisner, Th. Frauenheim, M. R. Manaa, *J. Chem. Phys.*, **117**, 788 (2002).
- [28] H. V. Brand, R. L. Rabie, D. J. Funk, I. Diaz-acosta, P. Pulay, and T. K. Lippert, *J. Phys. Chem. B*, **2002**, 10594 (2002).
- [29] A. Strachan, A. C. T. van Duin, D. Chakraborty, S. Dasgupta, and W. A. Goddard III, *Phys. Rev. Lett.*, **91**, 98301 (2003).
- [30] T. D. Sewell and R. Menikoff, *J. Chem. Phys.*, **119**, 7417 (2003).
- [31] C. K. Gan, T. D. Sewell, and M. Challacombe, *Phys. Rev. B* **69**, 035116 (2004).
- [32] R. Menikoff and T. D. Sewell, *Combustion Theory and Modelling*, **6**, 103 (2002).